

Forecasting future instability hazards at Anak Krakatau volcano, Indonesia, using archival reconstructions of edifice evolution

Kerys Meredew^{*1}, Sebastian F.L. Watt¹, Mike Cassidy¹, Achmad Fakhru Shomim², Muhammad Edo Nurshal^{3, 4}, Mirzam Abdurrahman⁴, Muhammad Hanif^{2, 5}, Wilfridus F.S. Banggur², Dini Nurfitriani², Samantha Engwell⁶, Victoria C. Smith⁷, Chiara M. Petrone⁸, Carl T.E. Stevenson¹ and Devy Kamil Syahbana⁹

¹ School of Geography, Earth and Environmental Sciences, University of Birmingham, Edgbaston, Birmingham, UK

² Research Center for Geological Disaster, National Research and Innovation Agency (BRIN), Bandung, Indonesia

³ Department of Geosciences, Penn State University, Pennsylvania, USA

⁴ Faculty of Earth Sciences and Technology, Bandung Institute of Technology, Bandung, Indonesia

⁵ Geospatial Imaging and Information Research Group (GI2RG), Faculty of Built Environment and Surveying, Universiti Teknologi Malaysia, Malaysia

⁶ British Geological Survey, The Lyell Centre, Edinburgh, UK

⁷ Research Laboratory for Archaeology and the History of Art, School of Archaeology, University of Oxford, Oxford, UK

⁸ Volcano Petrology Group, Natural History Museum, Cromwell Road, London, UK

⁹ Center for Volcanology and Geological Hazard Mitigation, Geological Agency, Ministry of Energy and Mineral Resources of Indonesia, Bandung, Indonesia

* kxm574@student.bham.ac.uk [corresponding author]

Online Resource 3: Extended Methodology

Within this document is additional information on:

1. Estimating the uncertainty introduced during the topographic reconstruction and Digital Elevation Model (DEM) generation processes
2. Details on the drone mapping and data processing involved in acquiring the June 2023 DEM
3. Exploration of uncertainty in projecting future edifice morphology

The DEMs used within the main paper can be downloaded here: <https://doi.org/10.5281/zenodo.17284993>

1. Estimating reconstruction uncertainty

Several areas of potential uncertainty are introduced during the topographic reconstruction and Digital Elevation Model (DEM) generation process, including via the digitised resolution, the method of interpolation, the data point positioning and the original map quality. To quantify this processing uncertainty, we use five higher-quality topographic maps to test the influence of digitisation, map quality and interpolation method on the final volumetric calculations. These maps are from April 1929 (Stehn, 1929b), August 1935 (Stehn, 1935), October 1941 (De Neve, 1951), August 1947 (De Neve, 1951) and October 1953 (Decker and Hadikusumo, 1961), and represent periods where Anak Krakatau had varied size, morphology and degrees of erosional flank gullying. The total estimated uncertainty margin for each DEM is summarised at the end of this section (Table S3).

Our analysis demonstrates that whilst different analytical decisions will (minimally) alter the calculated volume, the major source of uncertainty is the *unquantifiable* accuracy of the original maps. However, as the maps can be independently analysed, and exhibit self-consistent long-term growth patterns, we conclude that they are sufficiently accurate to not introduce any significant systematic error into the calculated growth rates.

1.1 How does the digitised resolution influence volumetric calculations?

Topography is digitised by manually plotting elevation points (in metres) along mapped contour lines to generate a GeoPackage point file (.gpkg). When all contours on a topographic map can be digitised, we define the resulting DEM as having a 100% digitised resolution. However, achieving this resolution is limited by the ability to trace all individual contour lines with certainty. The quality of contours varies considerably across our dataset; in some cases, printing and reproduction errors have resulted in image distortions, and in others the tight spacing of lines has resulted in specific contours becoming indistinguishable.

Measuring this impact on the volumetric calculations is therefore not only important for determining the minimum resolution required, but also for quantifying the potential error incurred when 100% resolution is not met. To assess this influence, contours from the five test maps were successively removed in increments of 25%. At each interval a DEM was generated (using Sibson interpolation), representing 0-100% resolution, and volumes were then calculated from these DEMs. For each DEM, both the basal contour (0 m) and the highest given contour or point (map dependent) were excluded from removals, keeping the respective island extents constant; when only these two contours remain, the digitised resolution is defined as 0%.

As contours were incrementally removed, the surface morphology of each DEM became less detailed, particularly reducing the number and complexity of erosive gullies on the outer flanks (Fig. S3.1). In cross section, this reduction in resolution also increased the step-like nature of the slope profiles, producing a series of flat terraces (Fig. S3.1). Overall, the resulting calculated volumes showed a minimal decrease between 100% and 25% resolution across all DEMs, except for April 1929, which marginally increased at 75% resolution (Table S3.1). At a digitised resolution of 75%, the calculated volumes decreased by an average of 0.18% (relative to 100% resolution), and then by 0.51% and 2.16% at 50 and 25% resolution, respectively. When reduced to 0% resolution, the DEMs retained no visual resemblance to the edifice (Fig. S3.1), with volumes decreasing by an average of 46.77%.

Of our 29 reconstructed maps, 15 could be digitised using all contours. The remainder could all be digitised to at least 75% resolution and the volumes derived from them have thus been assigned an uncertainty margin of $\pm 0.18\%$. However, this assessment is based on maps having contour spacings of ≤ 5 m; six of our reconstructed maps are of lower quality and have contours at intervals of > 5 m (Table S3.3). To address this, we assume a lower digitised resolution, calculated relative to if the map had contours at 5 m. For example, the January 2019 topographic map has contours at 10 m spacings, resulting in a resolution of 05%, and therefore we assume a volume uncertainty of $\pm 0.51\%$.

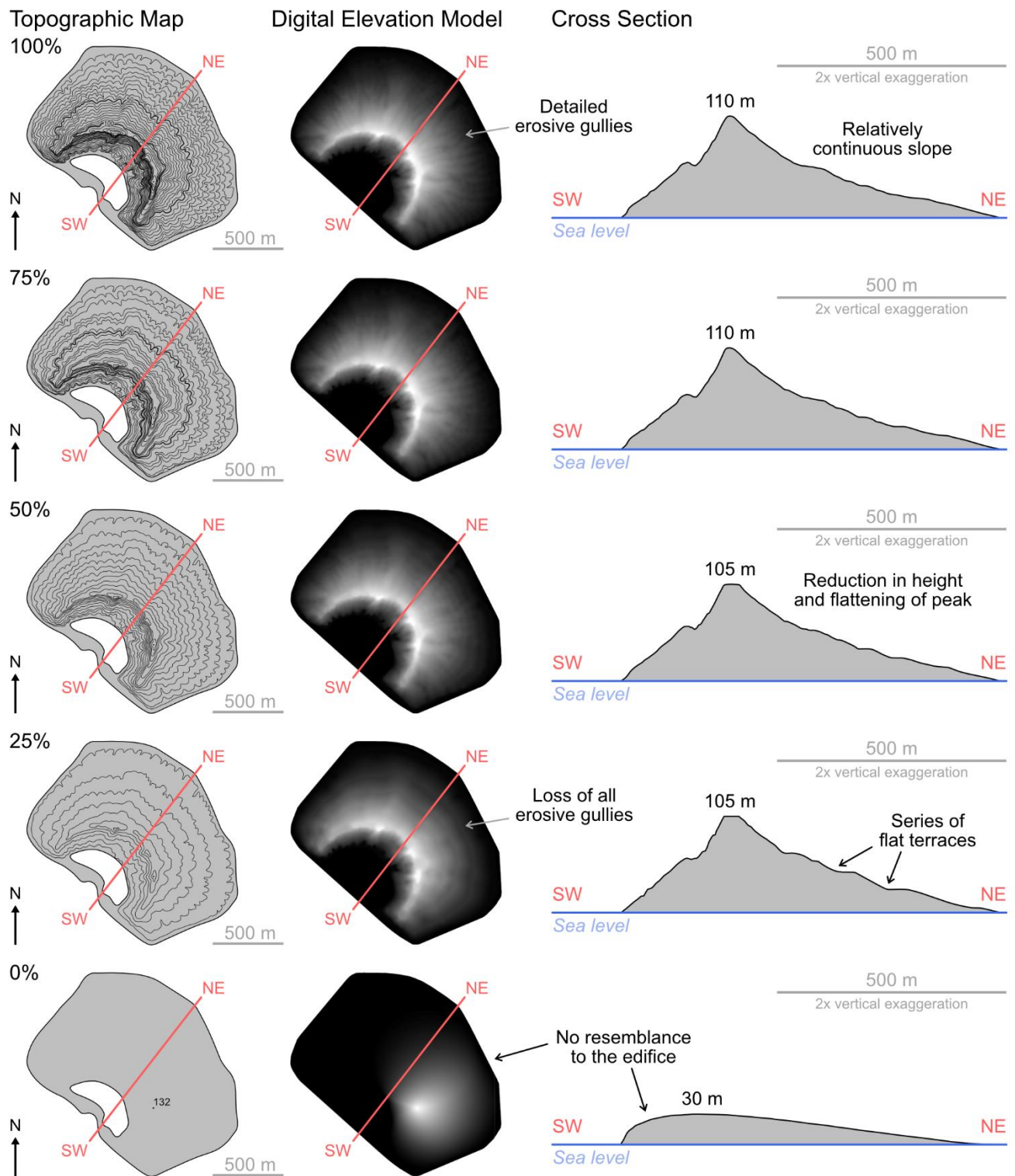


Fig. S3.1 Topographic maps, reconstructed DEMs and cross section profiles (SW-NE) of August 1947 at 0-100% digitised resolution. As contours are removed, the DEMs become less detailed and slopes profiles become increasingly stepped, producing a series of flat terraces and reducing the island height. All topographic maps and DEMs are of the same scale and orientation. At 100% digitised resolution the contours are at 5 m intervals. At 0% resolution, only 0 m and the highest point (132 m) remain.

Table S3.1 Volumes (m³) calculated for each of the five test maps, using DEMs generated by incrementally removing contours at intervals of 25%. When all contours are digitised, the resolution is defined as 100%, at 0% resolution only the basal contour (0 m) and highest contour/point remain.

Topographic Map	100%	75%	50%	25%	0%
April 1929	256319.53	256742.36	255065.74	247429.91	190206.85
Aug 1935	16574645.21	16552763.17	16472970.52	16007550.64	9932126.23
Oct 1941	53247203.87	53116604.72	52926374.89	52276018.18	24751119.22
Aug 1947	48147918.55	48044988.23	47877957.07	47506255.99	23251173.67
Oct 1953	81129472.53	81002728.58	80916955.57	80533047.06	30202330.79

1.2 To what extent does the DEM generation parameters influence the results?

Each reconstructed DEM is generated from a corresponding .gpkg point file using the SAGA Natural Neighbour interpolation module (Conrad et al., 2015). This method is used for grid interpolation from irregularly distributed points, outputting a continuous surface (the DEM), whilst also preserving input data values. When using this tool, the user must define the interpolation method as either: [0] Linear, [1] Sibson or [2] Non-Sibsonian, where Sibson interpolation is the default setting. Each method will produce a (slightly) modified version of the DEM, which in turn will impact the final volumetric calculation. Evaluating this influence is therefore necessary in determining how the interpolation method affects the reconstructed topography.

For each test map, we generated a separate DEM for each of the three different interpolation methods and compared the resulting calculated volumes (Table S3.2). All inputted .gpkg points files were digitised to 100% resolution. The DEMs produced via the Linear approach resulted in the highest volume estimates across all five maps. The Non-Sibsonian approach produced the lowest volume estimates, with the exception of April 1929. However, the overall variation in volumes between the techniques was negligible, differing from Sibson by an average of +0.038% for Linear and -0.016% for Non-Sibsonian, respectively. Visually, the Sibson approach produced the smoothest overall surface, maintaining the most continuous slopes (with fewer abrupt changes in surface morphology). This difference became more apparent at lower digitised resolutions (Fig. S3.2).

As a result, we determine Sibson interpolation provides a more realistic representation of the topography and have therefore selected it as our preferred interpolation approach. However, to account for any potential variation, each of our reconstructed volume estimates are applied with an interpolation method uncertainty margin of $\pm 0.038\%$.

Table S3.2 Volumes (m³) calculated for each of the five test maps, using DEMs generated via the three different methods of interpolation.

Map	Sibson	Linear	Non-Sibsonian
April 1929	256319.53	256487.92	256356.44
Aug 1935	16574645.21	16580779.24	16568276.58
Oct 1941	53247203.87	53269418.30	53233564.70
Aug 1947	48147918.55	48168321.84	48136111.15
Oct 1953	81129472.53	81133685.16	81125839.91

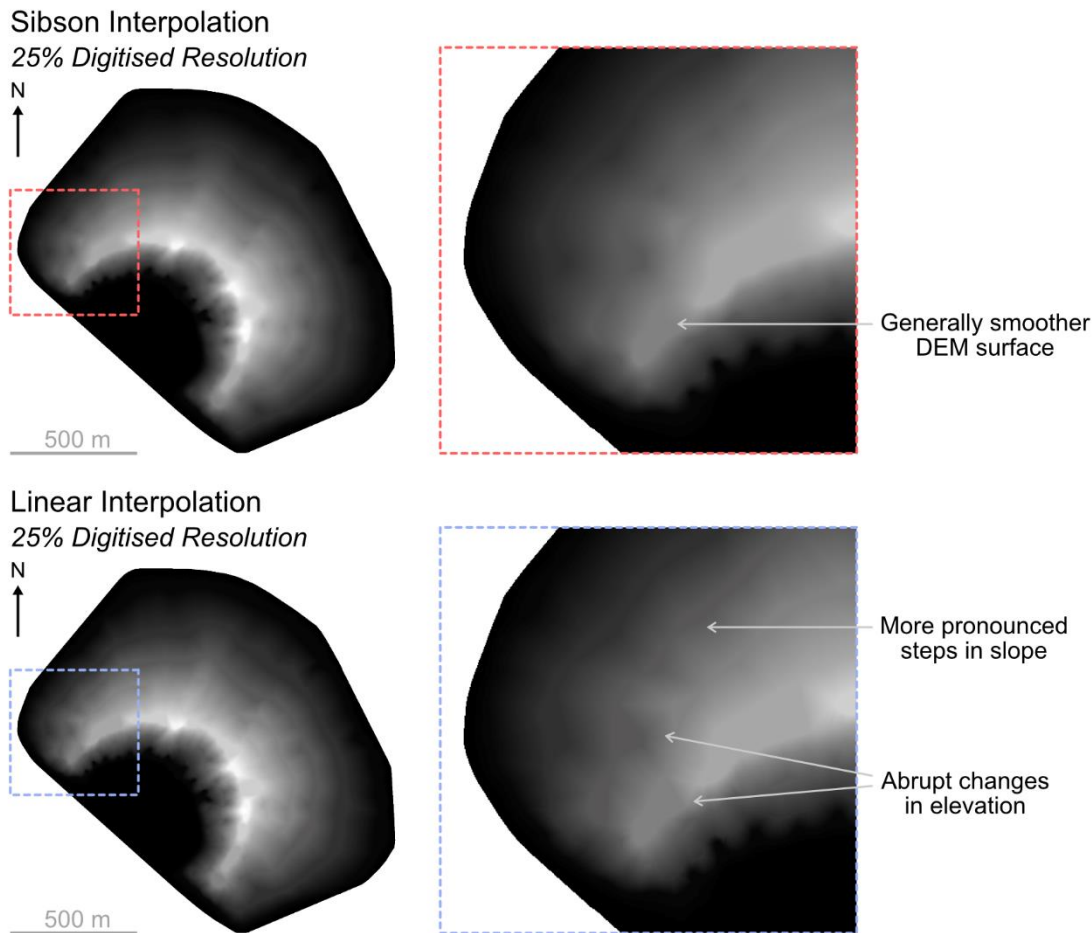


Fig. S3.2 Visual comparison of DEMs produced via Sibson and Linear interpolation methods (at 25% digitised resolution), using August 1947 as an example. The DEM generated using the Linear approach contains more pronounced steps in slope and areas of abrupt changes in elevation.

1.3 Does the version of QGIS influence results?

QGIS is an open-source software which follows a consistent scheduled development cycle, with an updated release published quarterly. The version used within this work (3.28.2 Firenze) was released in 21/10/2020 and is now out-dated. Testing whether volumetric results vary depending on the software version is therefore essential in verifying this method's repeatability.

To evaluate this influence, DEMs were produced for each of the five test maps using three different versions of QGIS: 3.28.2 Firenze, 3.16.2 Hannover (released 23/10/2020) and 3.8.2 Zanzibar (released 21/06/2019). Each inputted .gpkg file was digitised to 100% resolution, and method of interpolation defined as Sibson. Volume was then calculated from each DEM using the same respective software. Version 3.28.2 Firenze was set as the control, with the other two versions compared to this.

Results showed there was no variation in outputted volumes across the three tested software iterations. This method is therefore presumed repeatable regardless of QGIS version.

Table S3.3 Topographic, bathymetric, satellite- and drone-derived data sources used to reconstruct Anak Krakatau’s growth history from 1919-2023. The contour spacing (m), digitised resolution (%) and total estimated uncertainty (%) for each of the reconstructed DEMs is also included. DEMs are available for download: <https://doi.org/10.5281/zenodo.17284993>

Date of Survey	DEM File Name	Data Type	Contour Spacing (m)	Digitised Resolution	Total Applied Uncertainty	Source
1919	1919_Bathymetry	Digitised bathymetric survey	20-50	100%	Not quantified	Escher, 1919; Stehn, 1929a
10/04/1929	1929_April	Digitised topographic survey	2.5	100%	±0.038%	Stehn, 1929b
01/07/1930	1930_July	Digitised topographic survey	50	100%	±46.735%	Stehn, 1930
15/08/1930	1930_Aug	Digitised topographic survey	8.93	100%	±2.195%	Stehn, 1930
02/03/1933	1933_March	Digitised topographic survey	2.5	100%	±0.038%	Stehn, 1933a
17/10/1933-18/10/1933	1933_Oct	Digitised topographic survey	2.5	78.39%	±0.220%	Stehn, 1933b
07/02/1935-08/02/1935	1935_Feb	Digitised topographic survey	5	78.95%	±0.220%	Stehn, 1935
07/08/1935-09/08/1935	1935_Aug	Digitised topographic survey	5	100%	±0.038%	Stehn, 1935
11/12/1935-14/12/1935	1935_Dec	Digitised topographic survey	5	85.71%	±0.220%	Stehn, 1936a
14/06/1936-18/06/1936	1936_June	Digitised topographic survey	5	85.71%	±0.220%	Stehn, 1936b
14/08/1936-15/08/1936	1936_Aug	Digitised topographic survey	5	84.62%	±0.220%	Stehn, 1936c
11/12/1936-12/12/1936	1936_Dec	Digitised topographic survey	3	100%	±0.038%	Stehn, 1937a

Date of Survey	DEM File Name	Data Type	Contour Spacing (m)	Digitised Resolution	Total Applied Uncertainty	Source
13/02/1937-14/02/1937	1937_Feb	Digitised topographic survey	3	100%	±0.038%	Stehn, 1937b
17/12/1937-21/12/1937	1937_Dec	Digitised topographic survey	5	94.12%	±0.220%	Stehn, 1938
10/06/1938-13/06/1938	1938_June	Digitised topographic survey	5	82.35%	±0.220%	Neumann van Padang, 1938
12/08/1938-15/08/1938	1938_Aug	Digitised topographic survey	5	83.33%	±0.220%	Neumann van Padang, 1939
17/10/1938-19/10/1938	1938_Oct	Digitised topographic survey	5	78.95%	±0.220%	Stehn, 1939a
15/06/1939-17/06/1939	1939_June	Digitised topographic survey	5	78.95%	±0.220%	Stehn, 1939b, 1939c
16/08/1939-18/08/1939	1939_Aug	Digitised topographic survey	5	79.17%	±0.220%	Stehn, 1940
16/12/1940-17/12/1940	1940_Dec	Digitised topographic survey	5	80.77%	±0.220%	Van Bemmelen, 1941
09/10/1941-10/10/1941	1941_Oct	Digitised topographic survey	5	100%	±0.038%	De Neve, 1951
21/08/1947	1947_Aug	Digitised topographic survey	5	100%	±0.038%	De Neve, 1951
18/09/1950-19/09/1950	1950_Sept	Digitised topographic survey	5	79.31%	±0.220%	Decker and Hadikusumo, 1961
16/10/1952	1952_Oct	Digitised topographic survey	5	100%	±0.038%	Decker and Hadikusumo, 1961
11/10/1953-22/10/1953	1953_Oct	Digitised topographic survey	5	100%	±0.038%	Decker and Hadikusumo, 1961
12/01/1960-13/01/1960	1960_Jan	Digitised topographic survey	5	100%	±0.038%	Decker and Hadikusumo, 1961

Date of Survey	DEM File Name	Data Type	Contour Spacing (m)	Digitised Resolution	Total Applied Uncertainty	Source
March 1963	1963_March	Digitised topographic survey	2.5-20	100%	$\pm 0.220\%$	Zen and Hadikusumo, 1964
August 1985	1985_Aug	Digitised topographic survey	5-25	100%	$\pm 2.195\%$	Thornton and Rosengren, 1988
1990	1990	Digitised topographic survey	25	100%	$\pm 2.195\%$	Partomihardjo et al., 1992
21/09/1990-15/10/1990	Not provided	Bathymetric survey	N/A	N/A	Not quantified	Deplus et al., 1995
2012	Not provided	Satellite-derived DEM	N/A	N/A	Not quantified	Badan Informasi Geospasial (BIG), 2012
01/12/2018	Not provided	Adapted satellite	N/A	N/A	Not quantified	Gouhier and Paris, 2019; Grilli et al., 2021
22/12/2018	2018_Dec_Post-Col	Resected pre-collapse DEM	N/A	N/A	Not quantified	This paper.
10/01/2019	2019_Jan	Digitised topographic map	10	100%	$\pm 0.544\%$	Gouhier and Paris, 2019
01/08/2019	2019_Aug	Drone-derived DEM	N/A	N/A	Not quantified	BRIN and ITB.
12/08/2019-19/08/2019	Not provided	Bathymetric survey	N/A	N/A	Not quantified	Hunt et al., 2021
26/06/2021	2021_June	Drone-derived DEM	N/A	N/A	Not quantified	BRIN and ITB.
11/06/2022-13/06/2023	2023_June	Drone-derived DEM	N/A	N/A	Not quantified	This paper.

2. Drone mapping and data processing

An Unmanned Aerial Vehicle (UAV) survey was carried out in June 2023 (11/06/2023-13/06/2023), to provide an additional post-collapse datum, supplementing prior surveys from 2019 and 2021. Flights were conducted at a consistent altitude of ~375 m, along multiple autonomous flight paths, covering approximately 333 hectares, using a DJI Phantom 4 Pro equipped with a DJI 1-inch CMOS sensor. Most imagery was captured in nadir orientation, complemented by oblique photos from peripheral flight lines to improve surface reconstruction around steep slopes. Each image had a resolution of 4864×3648 pixels, taken with a 9 mm focal length (35 mm equivalent: 24 mm), f/10 aperture, 1/120 second shutter speed, and ISO-100. Forward and side overlaps were maintained at approximately 80% and 70%, respectively, to ensure robust photogrammetric performance (Westoby et al., 2012).

Processing was conducted using Agisoft Metashape Pro software and followed a typical Structure-from-Motion workflow, including image alignment, point cloud generation (sparse and dense), mesh building, texturing, DEM and orthomosaic production, and quality control (Seitz et al., 2006; Furukawa and Hernández, 2015). High-accuracy settings were applied throughout to retain surface detail and spatial precision. Spike noise in the initial DEM was addressed through manual inspection and filtered using a median filter implemented in QGIS. The model was georeferenced using the drone's onboard GNSS, then further adjusted through visual alignment with high-resolution satellite imagery and OpenStreetMap (OSM) basemaps (Turner et al., 2014). Vertical calibration was refined using tidal level data from the Indonesian Geospatial Information Agency (BIG), particularly focusing on improving elevation accuracy in coastal and nearshore areas.

The final DEM and orthomosaic achieved a Ground Sampling Distance (GSD) of ~35.5 cm per pixel, offering significantly improved spatial detail compared to national datasets such as Indonesian National Elevation Model (DEMNAS) at 8 m resolution. Uncertainty in volume calculated directly from this DEM, alongside other drone- and satellite-derived DEMs within this study, is unquantified.

3. Projecting future instability

When compared to the 2018 pre-collapse edifice, Anak Krakatau's current profile remains far lower, with a significantly reduced SW flank gradient. Prior to collapse, the edifice was ~330 m in height, with an average SW flank gradient of ~27°; as of June 2023, the central pyroclastic cone was ~103 m, with an average SW flank gradient of ~7°. The SW coastline additionally now extends a further ~25 m offshore (in the direction of failure).

Our projections of when the volcano's SW flank could approach a comparable morphology (i.e. equivalent slope gradient) to the 2018 pre-collapse edifice are based on an estimation of future cone height. We use the measured basal distance of 706 m (from the SW shoreline to the central vent) and the pre-collapse slope angle of ~27° to project a future cone height of ~360 m. The total volume of a simplified half cone of this size would be ~93993698 m³. By subtracting the volume of material already within this half cone (based on clipping the June 2023 DEM), we can then calculate the additional volume required to produce this morphology. This is based on the assumption that all subsequent growth on the SW flank accumulates within this half cone, rather than accumulating as lava flows beyond its footprint. From this, we then project the timeframe in which this volume could accumulate using our two growth scenarios: (1) volumetric growth continues at the current rate (2019-2023) of 5.03×10^{-3} km³/yr, or (2) growth slows to the long-term historical rate (1960-2018) of 7.99×10^{-4} km³/yr.

However, our estimate of cone height is dependent on the basal radius of the edifice. Any further increases in the island's diameter would consequently increase our estimate of edifice height, and therefore also the volume. For example, if the edifice increased by an additional 25 m from June 2023 (to 725 m), this would increase the projected edifice height to ~380 m and volume to ~101747968 m³ (Table S3.4). The timeframe in which this morphology would be met, would therefore also be increased. This would also result in a corresponding

increase in the scale of the collapse (i.e. volume of failed portion), provided that the future failure follows the same constraints as the 2018 collapse. We explore the extent to which increasing the edifice’s basal radius (Fig. S3.3) influences the projected timeframe and volume of potential future instability of Anak Krakatau’s SW flank in Table S3.4.

It is also worth noting that any other alterations to the edifice’s morphology and future failure geometry, such as the slope angle at which collapse occurs, the direction of failure and the basal shape of the edifice will also impact volume calculations. However, these factors are not evaluated within this work. We additionally emphasise that future failure conditions are also subject to various other uncertainties, and the reduced gradient of the submarine flank in particular is likely to be important as a relative stabilising factor.

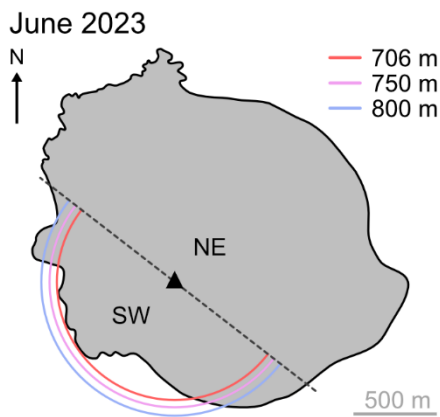


Fig. S3.3 Anak Krakatau’s shoreline morphology in June 2023, with example SW basal extents (red, pink and blue semi-circles) used in projecting future failure timeframes and volumes (Table S3.4). The location of the central pyroclastic cone is marked by the black triangle.

Table S3.4 Projected timeframes and volumes (m^3) of potential lateral collapse scenarios of Anak Krakatau’s SW flank, based on additional increases to the basal radius (m) of a simplified half cone. The volumetric growth rates of the SW sector used are: $5.03 \times 10^{-3} \text{ km}^3/\text{yr}$ (2019-2023) and $7.99 \times 10^{-4} \text{ km}^3/\text{yr}$ (1960-2018).

Basal Radius (m)	Projected cone height (m)	Projected simplified half cone volume (m^3)	Projected time based on 2019-2023 growth rates	Projected time based on 1960-2018 growth rates	Increase in volume of potential future collapse relative to 2018 failure (m^3)
706	360	93993698	2036	2104	41.65%
725	370	101747968	2038	2113	52.01%
750	382	112640745	2040	2126	66.86%
775	395	124284460	2042	2139	89.92%
800	408	136704145	2044	2154	100.20%

References

- Badan Informasi Geospasial (BIG). (2012). *DEMNAS National DEM* [DEM].
<https://tanahair.indonesia.go.id/demnas/###Info>
- Conrad, O., Bechtel, B., Bock, M., Dietrich, H., Fischer, E., Gerlitz, L., Wehberg, J., Wichmann, V. and Böhner, J. (2015). System for Automated Geoscientific Analyses (SAGA) v. 2.1.4. *Geoscientific Model Development*, 8(7), 1991–2007. <https://doi.org/10.5194/gmd-8-1991-2015>
- De Neve, G. A. (1951). Luchtverkenningen boven de vulkanen van Sumatra, Java en de Kleine Sunda Eilanden. *De Ingenieur in Indonesië*, 3(2), IV.13-IV.22.
- Decker, R. W., and Hadikusumo, D. (1961). Results of the 1960 expedition to Krakatau. *Journal of Geophysical Research (1896-1977)*, 66(10), 3497–3511. <https://doi.org/10.1029/JZ066i010p03497>
- Deplus, C., Bonvalot, S., Dahrin, D., Diamant, M., Harjono, H. and Dubois, J. (1995). Inner structure of the Krakatau volcanic complex (Indonesia) from gravity and bathymetry data. *Journal of Volcanology and Geothermal Research*, 64(1), 23–52. [https://doi.org/10.1016/0377-0273\(94\)00038-I](https://doi.org/10.1016/0377-0273(94)00038-I)
- Escher, B. G. (1919). Veranderingen in de Krakatau-groep na 1908 en wijzigingen in de opvatting van eenige geologische details. *Handelingen van Het Eerste Nederlandsch Indisch Natuurwetenschappelijk Congress, 3-6 October 1919*, 198–219.
- Furukawa, Y. and Hernández, C. (2015). Multi-View Stereo: A Tutorial. *Foundations and Trends® in Computer Graphics and Vision*, 9(1–2), 1–148. <https://doi.org/10.1561/06000000052>
- Gouhier, M. and Paris, R. (2019). SO₂ and tephra emissions during the December 22, 2018 Anak Krakatau flank-collapse eruption. *Volcanica*, 2(2), 91. <https://doi.org/10.30909/vol.02.02.91103>
- Grilli, S. T., Zhang, C., Kirby, J. T., Grilli, A. R., Tappin, D. R., Watt, S. F. L., Hunt, J. E., Novellino, A., Engwell, S., Nurshal, M. E. M., Abdurrachman, M., Cassidy, M., Madden-Nadeau, A. L. and Day, S. (2021). Modeling of the Dec. 22nd 2018 Anak Krakatau volcano lateral collapse and tsunami based on recent field surveys: Comparison with observed tsunami impact. *Marine Geology*, 440, 106566. <https://doi.org/10.1016/j.margeo.2021.106566>
- Hunt, J. E., Tappin, D. R., Watt, S. F. L., Susilohadi, S., Novellino, A., Ebmeier, S. K., Cassidy, M., Engwell, S. L., Grilli, S. T., Hanif, M., Priyanto, W. S., Clare, M. A., Abdurrachman, M. and Udrek, U. (2021). Submarine landslide megablocks show half of Anak Krakatau island failed on December 22nd, 2018. *Nature Communications*, 12(1), 2827. <https://doi.org/10.1038/s41467-021-22610-5>
- Neumann van Padang, M. (1938). Bulletin of the Netherland Indies Volcanological Survey. *Mining and Geological Department, Bandung*, 84.
- Neumann van Padang, M. (1939). Bulletin of the Netherland Indies Volcanological Survey. *Mining and Geological Department, Bandung*, 85.

- Partomihardjo, T., Mirmanto, E. and Whittaker, R. J. (1992). Anak Krakatau's vegetation and flora circa 1991, with observations on a decade of development and change. *GeoJournal*, 28(2), 233–248. <https://doi.org/10.1007/BF00177238>
- Seitz, S. M., Curless, B., Diebel, J., Scharstein, D. and Szeliski, R. (2006). A Comparison and Evaluation of Multi-View Stereo Reconstruction Algorithms. *2006 IEEE Computer Society Conference on Computer Vision and Pattern Recognition (CVPR'06)*, 1, 519–528. <https://doi.org/10.1109/CVPR.2006.19>
- Stehn, C. E. (1929a). Krakatau (Lang-Eiland, Verlaten-Eiland). *Bulletin of the Netherlands East Indian Volcanological Survey*, 20–21.
- Stehn, C. E. (1929b). *Krakatau: The geology and volcanism of the Krakatau group*. Proceedings of the Fourth Pacific Science Congress (Batavia).
- Stehn, C. E. (1930). *Bulletin of the Netherlands India Volcanological Survey*. 29–60(35–36).
- Stehn, C. E. (1933a). Bulletin of the Netherlands India Volcanological Survey. *Geological Survey, Bandung*, 29–60(60).
- Stehn, C. E. (1933b). Bulletin of the Netherlands Indies Volcanological Survey (Vol. III). *Mining and Geological Department, Bandung*, 61–74(62).
- Stehn, C. E. (1935). Bulletin of the Netherlands Indies Volcanological Survey (Vol. III). *Mining and Geological Department, Bandung*, 61–74(73).
- Stehn, C. E. (1936a). Bulletin of the Netherland Indies Volcanological Survey. *Mining and Geological Department, Bandung*, 74.
- Stehn, C. E. (1936b). Bulletin of the Netherland Indies Volcanological Survey. *Mining and Geological Department, Bandung*, 76.
- Stehn, C. E. (1936c). Bulletin of the Netherland Indies Volcanological Survey. *Mining and Geological Department, Bandung*, 77.
- Stehn, C. E. (1937a). Bulletin of the Netherland Indies Volcanological Survey. *Mining and Geological Department, Bandung*, 78.
- Stehn, C. E. (1937b). Bulletin of the Netherland Indies Volcanological Survey. *Mining and Geological Department, Bandung*, 79.
- Stehn, C. E. (1938). Bulletin of the Netherland Indies Volcanological Survey. *Mining and Geological Department, Bandung*, 82.
- Stehn, C. E. (1939a). Bulletin of the Netherland Indies Volcanological Survey. *Mining and Geological Department, Bandung*, 86.

- Stehn, C. E. (1939b). Bulletin of the Netherland Indies Volcanological Survey. *Mining and Geological Department, Bandung*, 87.
- Stehn, C. E. (1939c). Bulletin of the Netherland Indies Volcanological Survey. *Mining and Geological Department, Bandung*, 88.
- Stehn, C. E. (1940). Bulletin of the Netherland Indies Volcanological Survey. *Mining and Geological Department, Bandung*, 89.
- Thornton, I. W. B. and Rosengren, N. J. (1988). Zoological expeditions to the Krakatau Islands, 1984 and 1985: General introduction. *Philosophical Transactions of the Royal Society of London. B, Biological Sciences*, 322(1211), 273–316. <https://doi.org/10.1098/rstb.1988.0126>
- Turner, D., Lucieer, A. and Wallace, L. (2014). Direct Georeferencing of Ultrahigh-Resolution UAV Imagery. *IEEE Transactions on Geoscience and Remote Sensing*, 52(5), 2738–2745. <https://doi.org/10.1109/TGRS.2013.2265295>
- Van Bemmelen, R. W. (1941). Bulletin of the Netherland Indies Volcanological Survey. *Mining and Geological Department, Bandung*, No. 91-94.
- Westoby, M. J., Brasington, J., Glasser, N. F., Hambrey, M. J. and Reynolds, J. M. (2012). ‘Structure-from-Motion’ photogrammetry: A low-cost, effective tool for geoscience applications. *Geomorphology*, 179, 300–314. <https://doi.org/10.1016/j.geomorph.2012.08.021>
- Zen, M. T. and Hadikusumo, D. (1964). Recent changes in the Anak-Krakatau volcano. *Bulletin Volcanologique*, 27(1), 259–268. <https://doi.org/10.1007/BF02597525>